ELSEVIER

Materials Science and Engineering A 386 (2004) 254–261

MATERIALS SCIENCE & ENGINEERING A

www.elsevier.com/locate/msea

Thermodynamic assessment of liquid composition change during solidification and its effect on freckle formation in superalloys

Zhengdong Long[a], Xingbo Liu[a,*], Wanhong Yang[b], Keh-Minn Chang[a], Ever Barbero[a]

[a] *Department of Mechanical and Aerospace Engineering, West Virginia University, Morgantown, WV 26506, USA*
[b] *Special Metals Co., Huntington, WV 25705, USA*

Received 17 July 2003; received in revised form 9 July 2004

Abstract

The solidification macrosegregation, i.e. freckle, becomes more and more concerned with ever increasing demand for the large ingot size of superalloys. The evaluation of freckle formation is very difficult because of the less understanding of freckle formation mechanism and complex solidification behaviors of multi-component superalloys. The macrostructure of typical Nb-bearing and Ti-bearing superalloys in horizontally directional solidification and vacuum arc remelting (VAR) ingots were investigated to clarify the freckle formation mechanism. The thermodynamic approach was proposed to simulate the solidification behaviors. The relative *Ra* numbers, a reliable criterion, of freckle formation for some alloys were obtained based on the results of thermodynamic calculations. This thermodynamic approach was evaluated through comparison of the calculations from semi-experimental results. The *Ra* numbers obtained by thermodynamic approach are in good agreement with the ingot size capability of the industry melting shops, which is limited mainly by freckle defects.
Published by Elsevier B.V.

Keywords: Thermodynamic; Macrosegregation; Freckle; Superalloys

1. Introduction

The rapid growth in demand for clean, reliable, affordable power across the world has caused strong reaction to develop next generation of gas turbine power system [1,2]. However, the exceptional large castings and ingots needed to fabricate turbine discs and buckets have been restricting the development of this new generation power system. The lager ingots and castings result in slower solidification rate for the existing casting facility. A slow cooling rate will dramatically increase the inhomogeneity of the chemical composition. A typical defect of this inhomogeneity is freckle [3,4].

Freckles are black spots rich in low melting point compounds [5,6]. They cannot be removed by any subsequent forging or high temperature homogenization treatment. The existence of freckles dramatically reduces the mechanical properties and cause unexpected fatal explosion of the gas turbines. Although many efforts [7–10] have been made concerning the mechanism and criterion of freckle formation, there are still many issues kept unclear, especially the freckle formation mechanism and tendency evaluation of vacuum arc remelting (VAR) and electro-slag remelting (ESR) solidification processes.

The freckle is caused by segregation of alloying elements during the solidification. Obviously, the solutes distribution coefficient (k), reactions among alloying elements and phases formation during the solidification have large effects on segregation. The density of alloying elements is usually different from the base metal, either lighter or heavier. This results in the interdendritic liquid density difference. Convective flow due to the density difference washes and melts away existing solid and freckle will be formed as a result [11,12].

The chemical composition has a large effect on freckle formation. Table 1 lists the typical commercial superalloys and their chemical composition used for gas turbine engines. Some alloys, for instance IN718 contain high level of Nb

* Corresponding author. Tel.: +1-304-2933111x2324; fax: +1-304-2936689.
E-mail address: xingbo.liu@mail.wvu.edu (X. Liu).

0921-5093/$ – see front matter. Published by Elsevier B.V.
doi:10.1016/j.msea.2004.07.038

Table 1
The nominal compositions of some commercial superalloys (wt.%)

Alloy	Ni	Fe	Cr	Co	Al	Ti	Nb	W	Mo	C	B
U720	Balance	–	16.0	15.0	2.5	5.0	–	1.3	3.0	0.015	0.02
Waspaloy	Balance	–	19.5	13.5	1.4	3.0	–	–	4.1	0.05	0.01
IN718	Balance	18.5	19.0	–	0.5	0.9	5.1	–	3.0	0.04	0.002
IN706	Balance	40.0	16.0	–	0.2	1.8	2.9	–	–	0.03	0.002
IN625	Balance	2.5	21.5	–	0.2	0.2	3.6	–	9.0	0.05	–

element, which has lighter density than base metal Ni. Some alloys, for instance U720 contain high level of Ti element, which has lighter density than base metal Ni. In this paper, the freckles in IN718 and U720 ingots were examined and discussed in this paper.

The upward directional solidification (DS) was usually used to investigate the freckle formation mechanism [13,14]. However, it is not suitable to explain the freckle formation during the VAR/ESR remelting processes because of the large difference of solidification conditions. Based on VAR/ESR solidification conditions, the horizontal directional solidification was used to simulate the freckle formation in VAR/ESR ingots. Obviously, the effect of interdendritic liquid density difference on freckle formation was more clearly investigated by this solidification method. In this paper, the macrostructure of two model alloys, which have similar composition to commercial IN718 and U720 alloy, were examined and the freckle formation mechanism was also discussed. The freckle in actual VAR solidification was also characterized.

Many efforts have been made to establishment the criteria to evaluate the freckle formation tendency. It is well accepted that freckle is caused by the instable flow of solutes enriched interdendritic liquid in the mushy zone during the solidification. Several criteria were proposed based on this theory, and these criteria were evaluated by Yang et al. [15]. One of the major differences involves the selection of the characteristic length scale and another difference involves the use of permeability [16,17]. The criterion given by Flemings and co-workers was found to predict the freckle formation satisfactorily. Rayleigh number (*Ra*), as given in Eq. (1), was derived from this criterion. In this equation, the driven force to form freckle is liquid density difference, which is caused mainly by solute redistribution and liquid temperature during solidification. The resistance force is the permeability of interdendritic liquid flow, which is affected mainly by liquid faction and dendritic structure:

$$Ra = g\frac{\Delta\rho\Pi}{v f_L}\frac{1}{R} \tag{1}$$

where $\Delta\rho$ is the liquid density difference, g the gravity, Π the permeability, v the liquid viscosity, f_L the liquid fraction, and R is the crystal growth speed. In this paper, only the compositional effect on freckle formation is discussed. The viscosity change during solidification is not considered in this paper due to no reliable data available. Meanwhile, from Refs. [18,19], it can be assumed that the viscosity does not vary significantly in the mushy zone temperature range for superalloys. Therefore, a simplified Eq. (2) was used to calculate the relative *Ra*:

$$Ra\,(\text{relative}) = \frac{\Delta\rho\Pi}{f_L} \tag{2}$$

However, the calculation of interdendritic liquid density difference is very difficult because of complex solidification behaviors for multi-component superalloys. The molar fraction additive method was usually used to calculate the liquid density difference, if the liquid molar fraction and temperature are known. The permeability calculation is also based on the liquid fraction as a function of temperature [15]. Therefore, the liquid composition and temperature during solidification are very critical for the relative *Ra* calculation. Experimental techniques include quantitative metallography, X-ray diffraction analysis, EDS microprobe measurements and specially designed differential thermal analysis (DTA) device capable of rapid quenching. The experimental approaches were proved to be very inconvenient and time-consuming because of huge and complex experiments [20]. In this paper, the thermodynamic simulation, which has been proved very effective and cost-saving, was proposed to assess the liquid composition and liquid temperature during the solidification.

2. Experimental method

The solidification of the model alloy RN902 and R4006A were carried out in a horizontal directional solidification furnace system. The ingots had a rectangular shape with a dimension of 220 mm × 140 mm × 20 mm. The alloys were melted in an induction furnace and poured into the crucible. Horizontal directional solidification was controlled by cooling from one side and heating from the other three sides. The chemical composition of the RN902 alloy is Ni–20Cr–18Fe–7Nb, which is similar to commercial IN718 alloy. The chemical composition of the R4006A alloy is Ni–16Cr–15Co–5Ti–2.5Al–3Mo, which is similar to commercial U720 alloy. The commercial IN718 alloy was melted by VIM plus VAR processing. The ingot diameter is 257 mm, and freckle specimen was cut from around mid-radius. The optical and scanning electron microscopes (SEM) were used to observe the macrostructure.

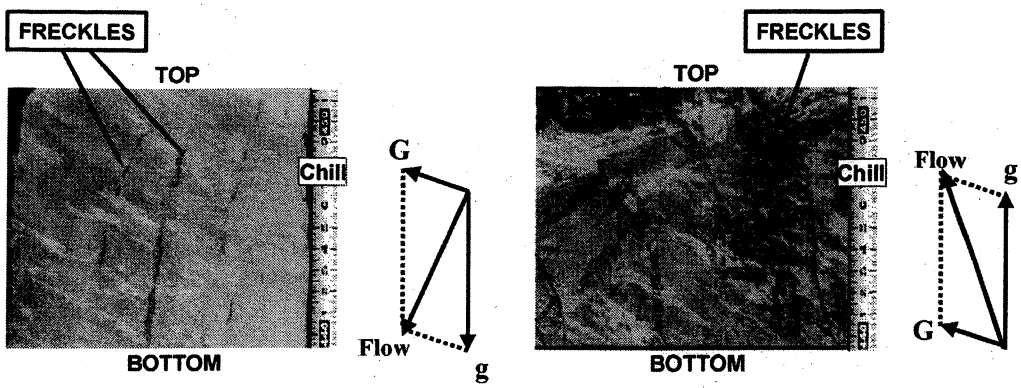

(a) RN902 alloy (b) R4006A alloy

Fig. 1. Macrostructure of RN902 and R4006A revealing freckles (G is the direction of thermal gradient, g the gravity and Flow is the interdendritic liquid flow direction).

3. Analytical approaches

3.1. Thermodynamic approach

Thermodynamic calculation through Gibbs energy is powerful to evaluate the state of existing phases. Based on the thermodynamics, the calculation of phase diagrams (CALPHAD) computational technique has been developed to calculate the phase equilibria and thermodynamic properties through Gibbs energy minimization approach [21,22]. For the multi-component alloy, the Gibbs energy is calculated based on the extrapolation of high-order properties from their lower-order binary and ternary systems which are available in literature. The following equation is general accepted to calculate the Gibbs energy [21]:

$$\Delta G = \sum_i x_i \Delta G_i^0 + RT \sum_i x_i \ln x_i + \sum_i \sum_{j>i} x_i x_j \sum_v \Omega_v (x_i - x_j)^v \quad (3)$$

where x_i is the mole fraction of the component i, ΔG_i^0 the free energy of the phase in the pure component i, T the temperature, R the gas constant, Ω_v is an interaction coefficient depending on the value of v. In practice the value of v lies between 0 and 2. Ternary interactions are often taken into account but there is little evidence of the need for considering the interaction terms which have a higher order than 3. Computational software to conduct the complicated calculation was developed. ThermoCalc^{TM} (Version N) was used to conduct the solidification simulation. Although the ThermoCalc^{TM} is only intended for equilibrium calculation, Scheil solidification simulation can be calculated by conforming to the local equilibrium assumption. The calculation starts with the nominal composition of the alloy and complete liquid phase in the system. By stepping with small decrement of temperature, we determine the new composition of the liquid. The solidification in the following step is calculated by resetting the new liquid composition as overall liquid composition. This method naturally treats the solidification with no solid diffusion and completely liquid diffusion. The outputs of Scheil module in ThermoCalc^{TM} include liquid composition, temperature, and thermodynamic variables such as Gibbs energy, activity, entropy, enthalpy, and specific heats. Obviously, the accurate description of solidification of an alloy relies on a reliable database that includes the contributions of individual element and interactions between multiple elements. The updated NiFe and Ni database have been used, which is proven to be adequate for most superalloys [23].

3.2. Semi-experimental method

The *Ra* calculation procedure is basically same for this approach as the one mentioned above, except the method to obtain the relationship of liquid composition and temperature. For the semi-experimental approach, the compositions in segregated sample were measured at a large number of different points. The solutes profiles were obtained by systematic point count techniques, and regression was performed to establish the relationship of liquid composition at different liquid fractions during the solidification. The liquid temperature was measured by differential thermal analysis (DTA).

4. Results and discussion

4.1. Macrostructure of freckle

Fig. 1 (a) and (b) gives the macrostructure of horizontally directional solidified (DS) alloy RN902 and R4006A in the longitudinal cross section. The chill side is on the right. It shows the grain growth direction, which is basically same with thermal gradient direction, is from right-bottom to top-left. The freckles in RN902 alloy are basically running from top to bottom but slightly leaning from right to left. For the

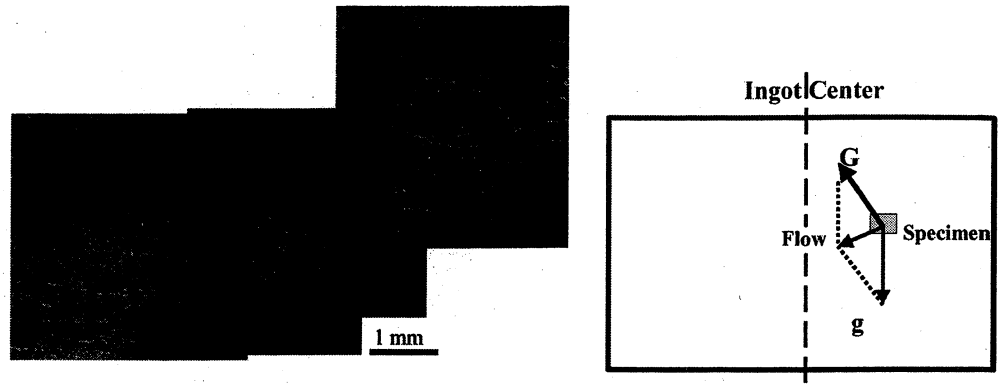

Fig. 2. Scanning electron micrography of freckle in IN718 VAR ingot (*G* is the direction of thermal gradient, *g* the gravity and Flow is the interdendritic liquid flow direction).

alloy R4006A, the freckles are basically running from bottom to top but slightly leaning from right to left. The obvious difference of freckle distribution for these two kinds of alloys can be seen.

Fig. 2 shows a freckle structure in IN718 VAR ingot and schematically the solidification conditions. Thermal gradient *G* points to up-center of melting pool while the gravity *g* points to bottom. The freckle is basically perpendicular to thermal gradient.

Freckle formation is directly associated with instable interdendritic fluid flow. The main factors to affect the fluid flow are thermal gradient and liquid density difference. The thermal gradient *G* determines grain growth direction and allows the liquid flow along the primary dendrite. On the other hand, due to solute elements partition during the solidification, the chemical composition of interdendritic liquid associated with dendrite bottom is different from that of the liquid associated with dendrite tip. Such liquid density difference causes interdendritic liquid flow and the flow may be upward if the dendrite-bottom liquid is lighter than dendrite-tip liquid. Figs. 1–3 schematically demonstrate the overall effect of thermal gradient and gravity on the interdendritic flow direction for horizontal DS and VAR. Therefore, the liquid density difference has a great effect on interdendritic liquid flow and freckle formation.

4.2. Thermodynamic approach to calculate the Ra number

4.2.1. Liquid composition and temperature

The relationship of liquid composition and temperature with the liquid fraction was calculated by ThermoCalc™ Scheil Simulation Module. Figs. 3 and 4 show the calculated results of IN718 and U720, as examples of typical Nb-bearing superalloy and Ti-bearing superalloy, respectively. The liquid composition has an obvious change during the solidification, which is the main reason for segregation and liquid density difference. The concentrations of some elements have a remarkable variation as the decrease of liquid fraction, but some have a minor variation. For example, the concentration of Nb in IN718 alloy increases dramatically as the liquid fraction decreases. Obviously, the higher the composition changes, the more the microsegregation is.

In Fig. 3, the concentrations of some elements change abruptly at certain liquid fraction. This is related to the new phase formation during the solidification. For instance Laves

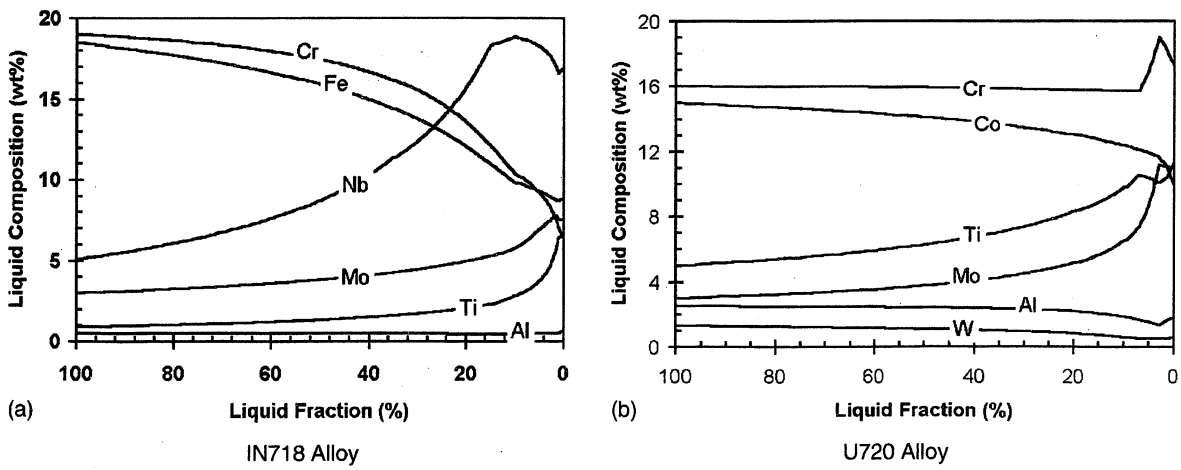

Fig. 3. Liquid composition as function of liquid fraction during the solidification.

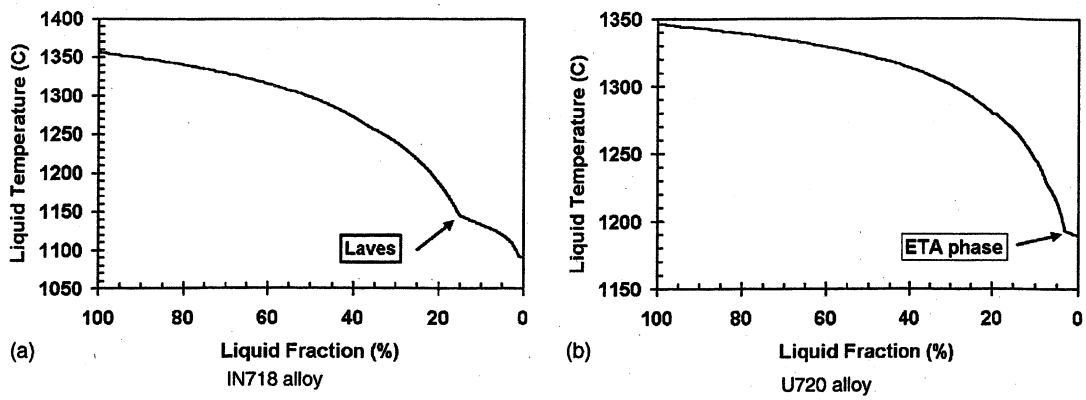

Fig. 4. Liquid temperature as function of liquid fraction during the solidification.

phase was predicted to occur when liquid fraction reaches 18% which is consistent with literature [24]. Therefore, the abrupt change of liquid composition appears at this liquid fraction. Phase formation also can be observed on the plot of liquid fraction versus liquid temperature in Fig. 4 (a) and (b).

4.2.2. Density difference during the solidification

The molar fraction additive method was used to calculate the liquid density. In order to increase the calculation correctness, the mixing molar volume (ΔV^{M}) was introduced by Sung the modified calculation showed a great reliability [25]:

$$\rho = \frac{\sum_i x_i A_i}{\sum_i x_i V_i + \Delta V^{M}} \tag{4}$$

where ρ is the liquid density, x_i, A_i and V_i the molar fraction, atomic weight and molar volume of an element. The x_i, V and ΔV^{M} can be calculated by the following equations:

$$x_i = \frac{C_i/A_i}{\sum C_i/A_i} \tag{5}$$

$$V = V_0[1 + (T - T_0)\alpha_l] \tag{6}$$

$$\Delta V^{M} = d_0 + d_1 X_1 + d_2 X_2 + d_3 X_3 \tag{7}$$

where T_0 is the melting temperature of the element, V_0 the molar volume at melting temperature, α_l the volume expansion coefficient in liquid status. The value of d_0–d_3 are listed in Table 2.

Fig. 5 shows the liquid density difference ($\Delta\rho$) based on the calculated results by thermodynamic approach. IN718 and IN625 have an obvious positive density difference and the values of $\Delta\rho$ increases as the liquid fraction decreases. U720 and Waspaloy have negative density difference and the absolute values of $\Delta\rho$ also increases as the liquid fraction increases. IN706 has a small negative density difference at first then it turns to positive. The overall value $\Delta\rho$ of IN706 is much smaller than other alloys.

Obviously, the liquid density difference is closely related to the initial chemical composition and liquid composition variation during the solidification. Table 1 shows IN718 and IN625 contain high level of Nb and low level of Ti and Al elements, and Fig. 3 shows the concentration of Nb in the liquid increase dramatically as the liquid fraction decreases. Therefore, the density of Nb enriched liquid becomes heavier with the increase of solid fraction. On the contrary, the U720 alloy contains high level of Ti and no Nb element. Therefore, the Ti enriched liquid becomes lighter with the increase of solid fraction. For IN706 alloy, the content of both Nb and Ti are between IN718 and U720 alloy. As a result, the liquid density shows minor variation during the solidification.

There are some abrupt changes of density difference for some alloys, especially at the smaller liquid fraction.

Table 2
Parameters for calculation of mixing molar volume [25]

d_0	−1.4982
d_1	4.4759
d_2	5.1988
d_3	0.43473
X_1	Al
X_2	Cr, Ti
X_3	Mo, W, Ta, Nb, Re, Hf

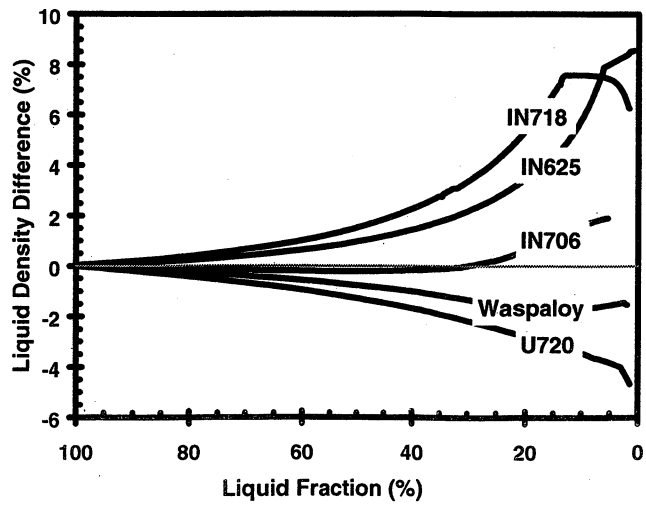

Fig. 5. Liquid density difference of several superalloys during solidification.

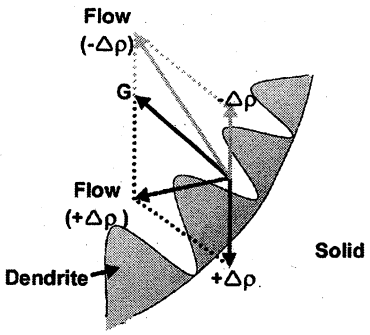

Fig. 6. The effects of thermal gradient and gravity on liquid flow direction in the mush zone of mid-radius VAR/ESR ingot.

Obviously, the abrupt change is related to a new phase formation during the solidification. For instance, the formation of Nb-enriched Laves phase will dramatically decrease Nb concentration in liquid phase, and the result is that the liquid density decreases rapidly.

4.2.3. Calculated results of Rayleigh number

The method to calculate the permeability used was initially proposed by Poirier [26], and then modified by Yang et al. [15]. Generally, the permeability can be calculated by Eq. (8) if the liquid flow along the primary dendrite arm. If the liquid flow perpendicularly to the primary dendrite arm, Eq. (9) can be applied to calculate permeability. There are basically two factors, i.e. thermal gradient and liquid gravity, to affect the interdendritic liquid flow direction, Fig. 6 shows schematically their effects on liquid flow direction. The flow direction will be affected seriously by gravity if the liquid density is positive and will be affected slightly if the liquid density difference is negative. This is consistent with experimental observations shown in Figs. 1 and 2. Therefore, the permeability was calculated by Eq. (9) for IN718 and IN625 alloys, and was calculated by Eq. (8) for U720 and Waspaloy. The IN706 alloy has a small negative liquid density difference at first and then it turns to positive. In order to give a comparative description of freckle formation tendency, the permeability of IN706 was calculated by Eq. (8) when it was compared with IN718 and IN625, and was calculated by Eq. (9) when it was compared with U720 and Waspaloy alloys:

$$\Pi = \frac{\Delta T}{\int_0^{\Delta T} f_L^{-2} dT} \tag{8}$$

$$\Pi = \frac{\Delta T}{\int_0^{\Delta T} f_L^{-3.34} dT} \tag{9}$$

Fig. 7 gives the calculated relative *Ra* numbers of IN718, IN625 and IN706. The positive value means that the liquid density difference is positive and negative value means that the liquid density difference is negative. The bigger the absolute value of *Ra* number is, the higher the freckle formation tendency is. The calculated results show that the IN718 alloy

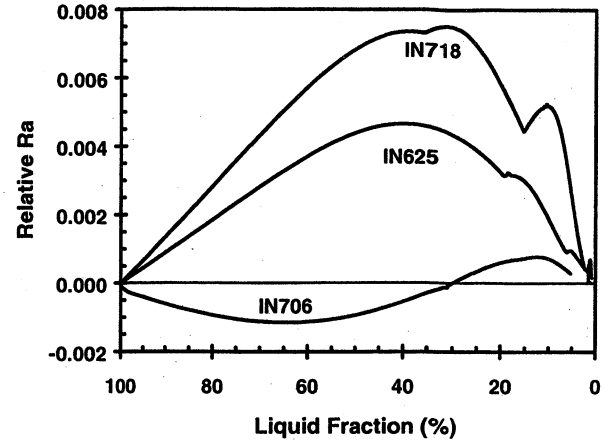

Fig. 7. *Ra* numbers of IN718, IN625 and IN706 alloys.

has the largest relative *Ra* number, and IN706 alloy has the lowest relative *Ra* number among these three alloys.

The tendency to form freckle in an alloy is related to maximum *Ra* number through solidification. The maximum value occurs at 0.4–0.6 liquid fraction. As liquid fraction decreases, the liquid density difference increases, but the permeability decreases. As a result, the maximum relative *Ra* number appears about 40–60% of liquid fraction.

There are some abnormal changes of the calculated *Ra* numbers in the lower liquid fraction. These abnormal changes are related to the abrupt changes of liquid density difference, which are usually caused by phase formation during the solidification. However, the overall value of relative *Ra* number is not very high at low liquid fraction because liquid flow permeability is dramatically decreased in low liquid fraction. The secondary phase formation, such as Laves, δ-Ni_3Nb and Carbide phases, has little effect on the freckle formation if the interdendritic secondary phase forms at the low liquid fraction.

Fig. 8 gives the calculated results of *Ra* numbers for U720, Waspaloy and IN706 alloys. The ascent sequence of absolute *Ra* number is IN706, Waspaloy and U720 alloys. It shows

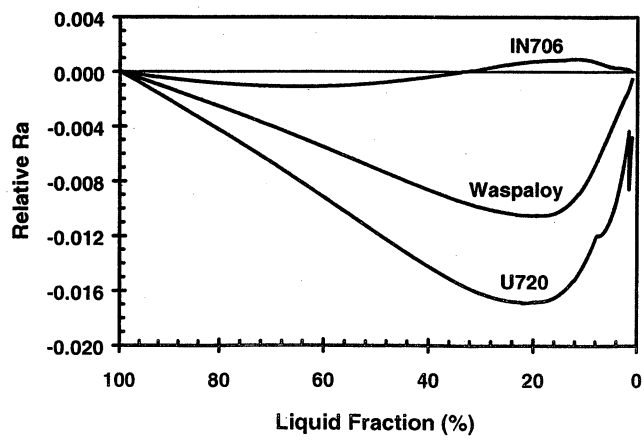

Fig. 8. *Ra* numbers of U720, Waspaloy and IN706 alloys.

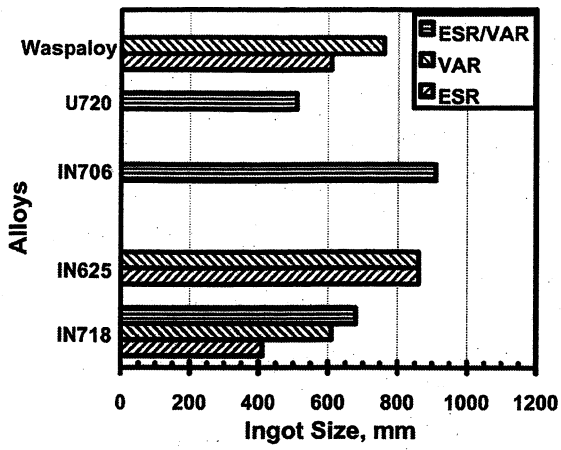

Fig. 9. Ingot size capability [23].

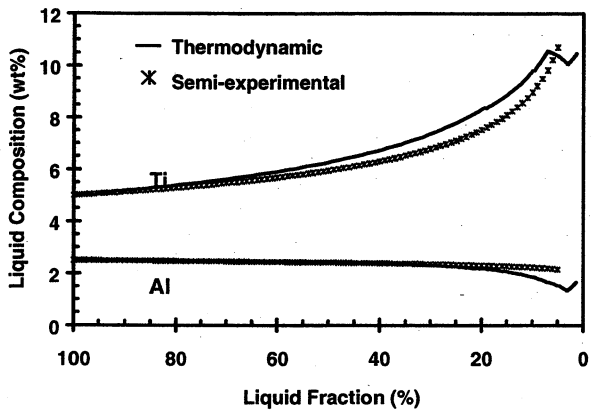

Fig. 10. Liquid composition calculated by thermodynamic and semi-experimental approaches.

the U720 is more prone to freckle formation than Waspaloy and IN706 alloys during solidification.

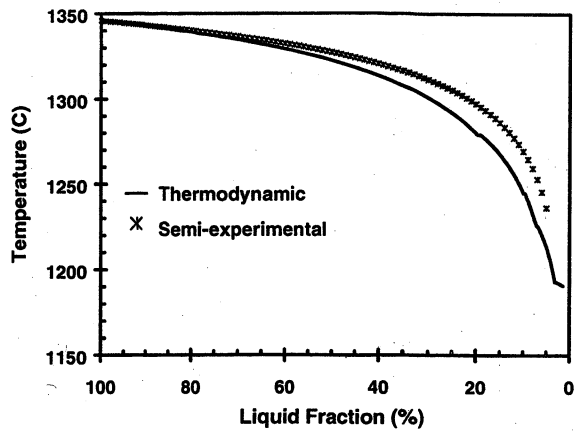

Fig. 11. Liquid temperature calculated by thermodynamic and semi-experimental approaches.

4.3. Evaluation of the thermodynamic approach

4.3.1. Ingot size capability of some commercial alloys

Fig. 9 gives the state-of-art ingot size capability of some superalloys in commercial melting shop [27]. The ingot size capability of IN625 is higher than that of IN718. The ingot size capability of Waspaloy is higher than that of U720 for the Ti-bearing superalloys. The IN706 has the highest ingot size capability among these alloys. It is well known that the ingot size capability is mainly limited by freckle formation. By comparing the ingot size capability in Fig. 9 to the calculated *Ra* number in Figs. 7 and 8, the calculated results of *Ra* number through thermodynamic approach is consistent with ingot size capability.

4.3.2. Comparison of thermodynamic and semi-experimental results

Figs. 10 and 11 give calculated results of liquid composition and liquid temperature of U720 by thermodynamic and semi-experimental approaches, respectively. It shows the

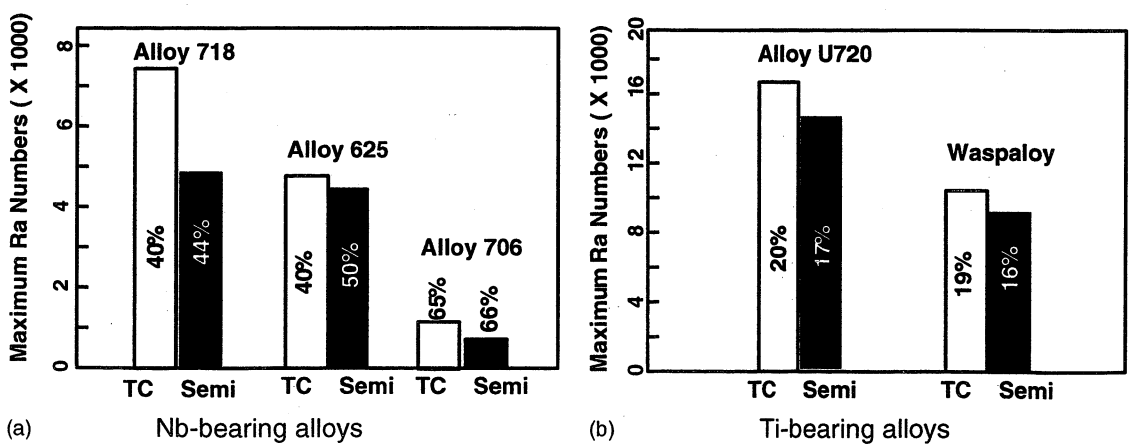

Fig. 12. Comparison of maximum *Ra* numbers by thermodynamic and semi-experimental approaches (the percentage is the liquid fraction at maximum *Ra* number).

results are basically close to each other for this alloy. Fig. 12 shows the maximum *Ra* numbers and corresponding liquid fraction for these alloys through thermodynamic and semi-experimental approaches. Because the equations to calculate permeability are different for Nb-bearing and Ti-bearing alloys, it is meaningless to compare the *Ra* numbers between these two types of alloys. There is minor difference for IN625, IN706, U720 and Waspaloy alloys for the two calculation approaches. Therefore, the thermodynamic approach shows good reliability to evaluate the freckle formation tendency. It also can be seen there is an obvious difference for IN718 alloy, this is related to the accurateness of database. It is suggested that a more accurate database concentrated on the solidification temperature range should be developed to offer the best benefits of thermodynamic modeling of freckle formation.

5. Summary

1. The solidification can be simulated by thermodynamic approach. ThermoCalc^{TM} coupling with its database can provide an effective approach to get liquid composition and temperature profiles during the solidification.
2. Relative Rayleigh (*Ra*) numbers of some wildly used superalloys were calculated based on this thermodynamic approach.
3. The results of thermodynamic simulation are basically similar to those of semi-experimental analysis. A good agreement was found with the capability of ingot size of the melting shop.

References

[1] P.W. Schilke, R.C. Schwant, in: E.A. Loria (Ed.), Superalloys 718, 625,706 and Derivatives, Pittsburgh, PA, 2001, pp. 1–12.
[2] R.C. Schwant, et al., in: E.A. Loria (Ed.), Superalloys 718, 625, 706 and Various Derivatives, TMS, 1997, pp. 141–152.
[3] W. Chen, Compositional Effects on Macroscopic Solidification Segregation of Superalloy, Ph.D. Dissertation, West Virginia University, 2000.
[4] A.F. Crawley, Int. Met. Rev. 19 (1974) 32–48.
[5] S.T. Wlodek, in: E.A. Loria (Ed.), Superalloys 718 625, 706 and Various Derivatives, TMS, 1994, pp. 167–176.
[6] A.D. Helms, C.B. Adasczil, L.A. Jackman, in: R.D. Kissinger, et al. (Eds.), Superalloys 1996, TMS, 1996, pp. 427–433.
[7] M.C. Flemings, et al., Trans. Metall. AIME 239 (1967) 1449–1461.
[8] M.C. Flemings, et al., Trans. Metall. AIME 242 (1968) 41–55.
[9] T.M. Pollock, et al., Metall. Trans. A 27A (1996) 1081–1094.
[10] P. Auburtin, et al., Metall. Trans. B 31B (2000) 801–811.
[11] R.J. McDonald, et al., Metall. Trans. 1 (1970) 1787–1788.
[12] C. Beckermann, JOM (1997) 13–17.
[13] T. Fujii, D.R. Poirier, M.C. Flemings, Metall. Trans. B 10B (1979) 331.
[14] R. Sellamuthu, H.D. Brody, A.F. Giamei, Metall. Trans. B 17B (1986) 347–358.
[15] W.H. Yang, W. Chen, K.-M. Chang, S. Mannan, J. deBarbadillo, Mater. Metall. Trans. 31A (2001) 397–406.
[16] C. Frueh, D.R. Poirier, R.G. Erdmann, S.D. Felicelli, Mater. Sci. Eng. A 345 (2003) 72.
[17] C. Frueh, D.R. Poirier, R.G. Erdmann, S.D. Felicelli, Mater. Sci. Eng. A 328 (2003) 245.
[18] M. Hirai, ISIJ Int. 33 (1993) 251–258.
[19] K.C. Mills, P.N. Quested, in: A. Mitchell (Ed.), Proceedings of the Conference on Liquid Metal Processing and Casting, AVS, 1994, pp. 226–240.
[20] W.H. Yang, W. Chen, K.-M. Chang, S. Mannan, J. deBarbadillo, Mater. Metall. Trans. A 31A (10) (2001) 2459–2464.
[21] N.Sauners, A.P. Miodownik, in: R.W. Cahn (Ed.), CALPHAD, Pergamon, 1998.
[22] B. Sundman, in: F.H. Hayes (Ed.), User Aspects of Phase Diagrams, 1991.
[23] B.A. Boutwell, in: E.A. Loria (Ed.), Superalloys 718, 625, 706 and Various Derivatives, TMS, 1997, pp. 99–106.
[24] S.T. Wlodek, in: E.A. Loria (Ed.), Superalloys 718 625, 706 and Various Derivatives, TMS, 1994, pp. 695–671.
[25] P.K. Sung, Mater. Sci. Eng. A A231 (1997) 189–197.
[26] D.R. Poirier, Metall. Trans. A 10A (9) (1988) 2349–2354.
[27] R. Kennedy, et al., in: K.-M. Chang, et al. (Eds.), Advanced Technologies for Superalloy Affordability, TMS, 2000, pp. 159–171.

R00080612 MSA 18246